1-1-2007

Manganese dioxide cathode in the presence of TiS2 as additive on an aqueous lithium secondary cell

Manickam Minakshi
Murdoch University

Pritam Singh
Murdoch University

David RG Mitchell
Institute of Materials and Engineering Science, ANSTO, dmitchel@uow.edu.au

Manganese dioxide cathode in the presence of TiS2 as additive on an aqueous lithium secondary cell

Abstract

Intercalation of lithium into the vacant sites of a host compound can be achieved electrochemically using nonaqueous electrolytes. The use of aqueous electrolyte is less common because of the reactivity of many lithium intercalation compounds with water. Here, we propose that lithium could be intercalated into the manganese dioxide cathode in a battery using saturated lithium hydroxide as the electrolyte. The positive electrode reaction at MnO2 in this medium is shown to be lithium insertion rather than the usual protonation, and acceptable rechargeability is observed. Using X-ray photoelectron spectroscopy and scanning electron microscope analysis on the discharged cathode material we confirmed the presence of lithium ions in the host structure of MnO2. Further, the incorporation of small amounts (<3 wt>%=weight percent) of titanium disulphide (TiS2) additive to the cell MnO2 cathode leads to a significant improvement in cell performance.

Keywords

cathode, cell, secondary, lithium, aqueous, dioxide, additive, manganese, tis2, presence

Disciplines

Engineering | Physical Sciences and Mathematics

Publication Details

Minakshi, M., Singh, P. and Mitchell, D. RG. (2007). Manganese dioxide cathode in the presence of TiS2 as additive on an aqueous lithium secondary cell. Journal of the Electrochemical Society, 154 (2), A109-A113.

Journal of The Electrochemical Society, **154** (2) A109-A113 (2007)
0013-4651/2006/154(2)/A109/5/$20.00 © The Electrochemical Society

Manganese Dioxide Cathode in the Presence of TiS_2 as Additive on an Aqueous Lithium Secondary Cell

Manickam Minakshi,[a,*,z] Pritam Singh,[a] and David R. G. Mitchell[b]

[a]*Division of Science and Engineering, Murdoch University, Murdoch, WA 6150, Western Australia*
[b]*Institute of Materials and Engineering Science, ANSTO, PMB 1, Menai, New South Wales 2234, Australia*

Intercalation of lithium into the vacant sites of a host compound can be achieved electrochemically using nonaqueous electrolytes. The use of aqueous electrolyte is less common because of the reactivity of many lithium intercalation compounds with water. Here, we propose that lithium could be intercalated into the manganese dioxide cathode in a battery using saturated lithium hydroxide as the electrolyte. The positive electrode reaction at MnO_2 in this medium is shown to be lithium insertion rather than the usual protonation, and acceptable rechargeability is observed. Using X-ray photoelectron spectroscopy and scanning electron microscope analysis on the discharged cathode material we confirmed the presence of lithium ions in the host structure of MnO_2. Further, the incorporation of small amounts (<3 wt % = weight percent) of titanium disulphide (TiS_2) additive to the cell MnO_2 cathode leads to a significant improvement in cell performance.
 [DOI: 10.1149/1.2403079]

Manuscript submitted July 4, 2006; revised manuscript received September 19, 2006. Available electronically December 21, 2006.

The demand for rechargeable batteries for a variety of applications, particularly in electronic devices, is constantly growing. An important aspect is the environmental threat posed by the heavy metals used in many of today's batteries proposed or in current use. Lithium batteries also pose environmental problems. In this regard, the lithium-ion battery "rocking chair" system is an obvious choice.[1] This battery now represents the state-of-the-art in small-size rechargeable cells for consumer electronic devices. The cathode material in this battery relies on the application of one of the well-known lithium insertion compounds $LiCoO_2$, $LiNiO_2$, $LiMn_2O_4$, or γ-MnO_2.[2-5] Insertion compounds are the ones in which the rigid host lattice of the compound remains unchanged after repeated insertion and extraction of lithium or any other foreign atoms. Recently, materials based on transition metal polyanions have also been proposed, and phosphate compounds crystallizing as Nasicon structures appear to hold particular promise[6,7] as a potential cathode material. For instance, it has been suggested that olivine-type lithium iron phosphate, $LiFePO_4$, may offer the optimal combination of low cost, favorable electrochemical activity, and low environmental impact.[8] It is widely reported that intercalation of lithium into the vacant sites of these insertion compounds has been achieved electrochemically using nonaqueous electrolytes-combination of solvents like ethylene carbonate, propylene carbonate, dimethyl carbonate, etc.[1-8] The use of aqueous methods is less common because of the reactivity of many lithium intercalation compounds with water. Lithium electrolytes in ambient temperature systems are typically dissolved in organic solvents or polymeric materials; both options limit the power density that can be achieved in comparison with aqueous electrolyte. Hence, in one of our previous studies[9] we reported that lithium could be intercalated into manganese dioxide from LiOH solution in an aqueous cell.

In traditional alkaline batteries using KOH as the electrolyte, MnO_2 is not suitable for its reversibility, because during discharge the electrode reaction involves the insertion of protons into the ionic lattice of the manganese dioxide according to the equation

$$MnO_2 + H^+ + e^- \rightarrow MnOOH \quad [1]$$

whereas the use of aqueous LiOH as an electrolyte results in the incorporation of lithium ions into the MnO_2 structure during the discharge[10,11]

$$Li^+ + e^- + MnO_2 \rightarrow LiMnO_2 \quad [2]$$

The overall reaction of the alkaline Zn/MnO_2 battery using LiOH electrolyte could be written as

$$xLi + H_2O + 2MnO_2 \rightarrow Li_xMnO_2 + MnOOH + OH^- \quad [3]$$

During cell discharge, Li^+ ions and protons are inserted into the MnO_2 structure, causing the reduction of Mn^{4+} ions to Mn^{3+} ions. During oxidation, the Li_xMnO_2 reverts to its original phase upon the extraction of Li^+ ions from the structure.[10,11]

The main objectives of this paper are to report on

1. Understanding the discharge mechanism in aqueous lithium hydroxide electrolyte via surface characterization using various physical techniques.
2. Improvement in cell performance by adding small amounts (<3 wt %) of titanium disulfide (TiS_2) to the cathode and its rechargeability.

Experimental

The γ-MnO_2 of battery grade material used in this work was purchased from Sigma Aldrich. Titanium disulfide (TiS_2) was obtained from Alfa Aesar. For the electrochemical test, a pellet was prepared by mixing 70–75 wt % MnO_2 consisting of 0–5 wt % TiS_2 with 20 wt % acetylene black (A-99, Asbury, USA) and 5 wt % poly (vinylidene difluoride) (PVDF, Sigma Aldrich) binder in a mortar and pestle. A Swagelok-type electrochemical cell[9,12] was constructed with the disklike pellet as the cathode, Zn metal as the anode, and filter paper (Whatman filters 12) as the separator. The electrolyte was a saturated solution of lithium hydroxide (LiOH) containing 1 mol L^{-1} zinc sulfate ($ZnSO_4$). The cells were discharged-charged galvanostatically at 0.3 mA/cm^2 by using an EG&G Princeton Applied Research potentiostat/galvanostat model 273 A, operated by model 270 software (EG&G). The cutoff discharge and charge voltages were 1.0 and 1.8 V, respectively. Reported potentials are relative to Zn metal. All electrochemical measurements were carried out at ambient atmosphere. The products formed during charge and discharge cycles were characterized by X-ray photoelectron spectroscopy (XPS) and scanning electron microscopy (SEM) techniques. XPS (Kratos Ultra Axis spectrometer) using monochromatic Al Kα (1486.6 eV) radiation was used to analyze the chemical binding energy of the samples. XPS analysis was started when the pressure in the analysis chamber fell below 1×10^{-9} hPa. Carbon, C (1s), was used as a reference for all the samples. The surface analysis of the materials was conducted by using a scanning electron microscope (Philips Analytical XL series 20).

Results and Discussion

Electrochemical behavior of MnO_2 in aqueous LiOH cell.— Figure 1 shows the discharge-charge characteristics of the

* Electrochemical Society Active Member.
z E-mail: minakshi@murdoch.edu.au

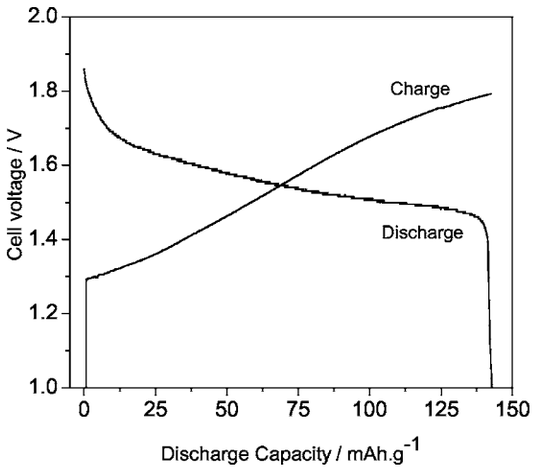

Figure 1. The first discharge-charge profile of Zn-MnO_2 cells using saturated aqueous LiOH containing 1 mol L^{-1} of $ZnSO_4$ as the electrolyte. The cathode is composed of MnO_2 (75 wt %), PTFE (10 wt %) as binder, and carbon black (15 wt %) for conductivity.

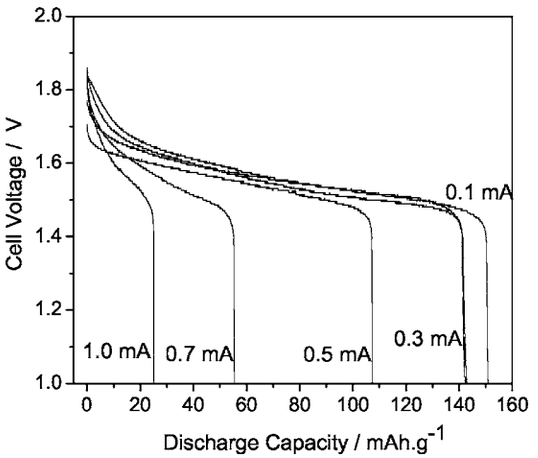

Figure 3. Effect of various discharge currents on the first discharge cycle for the Zn-MnO_2-aqueous battery.

Zn-MnO_2-aqueous lithium hydroxide cell. The cell was discharged and charged galvanostatically (0.3 mA/cm^2) to 1.0 and 1.8 V, respectively. On commencement of discharge, the voltage dropped from the open-circuit voltage (OCV) 1.85 to 1.7 V and then gradually decreased to 1.4 V. The discharge was terminated when the voltage suddenly fell to 1.0 V. The 1.6 V region could correspond to the $Mn^{4+}/^{3+}$ redox couple. The practically realizable capacity of the material is found to be 140 mAh/g. The percentage of material utilization was 50%. During the charge process, from 1.3 V there was a constant increase in potential up to the charge cutoff voltage of 1.8 V. As can be seen in Fig. 1, the cell could be reversibly discharged and charged.

The rechargeability of the cell Zn-MnO_2 was investigated and the results are shown in Fig. 2. The MnO_2 cathode could deliver a reversible capacity of about 138 and 110 mAh/g for the second and tenth cycles, respectively. After a few cycles the loss in capacity stabilized and the cell was able to deliver as many as 40 cycles with a discharge capacity of 70 mAh/g. The coulombic efficiency dropped rapidly during the first 20 cycles from 82 to 56%, after which the decrease was gradual. At the 40th cycle the efficiency was decreased to 45%. This behavior indicates that the material is rechargeable in aqueous solutions.

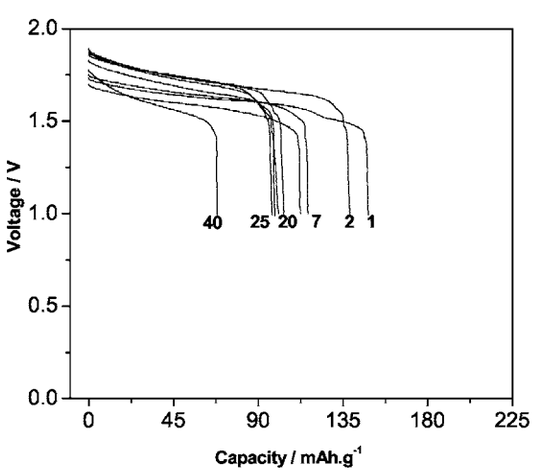

Figure 2. Discharge curves for various cycles illustrating the cyclability of MnO_2 samples.

In order to evaluate the effect of discharge current on the MnO_2 cathode in aqueous LiOH electrolyte, we performed the discharge process with various discharge currents between 0.1 and 1.0 mA, and their results are shown in Fig. 3. The observed discharge capacity at relatively low currents of 0.1, 0.3, and 0.5 mA is 150, 140, and 105 mAh/g. An increase in the current to 0.7 and 1.0 mA results in an important decrease of the discharge capacity from 150 to 55 and 25 mAh/g, respectively. In the discharge curve for higher current (0.5 mA) the $Mn^{4+}/^{3+}$ redox couple region was slightly shifted to a lower voltage. For the discharge current of 1.0 mA the $Mn^{4+}/^{3+}$ redox couple region has not been well observed within the cutoff voltage. This abrupt drop in voltage signals that a reduction of manganese is not complete. The capacity loss occurring at a high rate of discharge (0.7 and 1.0 mA) in Fig. 3 is not irreversible. The capacity is regained on returning to low discharge current of 0.1 and 0.2 mA, which shows that the loss of capacity is likely to be a kinetic effect.[13] Hence, the cell is able to sustain the discharge current limit of 0.5 mA.

Physical characterization of the discharged cathode material.— The cathode material formed during the discharge cycle was characterized by using physical techniques, i.e., SEM and XPS.

The morphology of the MnO_2 before and after discharge and recharged samples has been studied via SEM. Examination of the surface of MnO_2 uncycled cathode via SEM (Fig. 4a) revealed that the particle size is of the order of 20–25 μm. On discharge, Fig. 4b, the micrograph shows a different morphology with the particle size of the order 40–50 μm. It appears that during discharge the original MnO_2 particles agglomerate into larger particles perhaps containing lithium ions intercalated into the material. On recharge, Fig. 4c, the micrograph shows the absence of this agglomeration. However, the structural irreversibility of the starting MnO_2 is observed in the morphology, and is most likely the reason for the loss in cell capacity after various cycles, as shown in cycling behavior, Fig. 2.

Due to the low crystallinity of the starting material, the X-ray diffraction (XRD) pattern showed only broad Bragg reflections. The discharged cathode was covered with a thick layer of materials (as explained in this section). Therefore, XRD is not a suitable technique for aqueous LiOH solutions. Hence, in order to confirm the existence of lithium ions in the solid matrix of the discharged cathode material, it was subjected to powerful tools for surface studies, i.e., XPS and secondary-ion mass spectrometry (SIMS) studies. The surface of the cathode material was ion bombarded to remove the

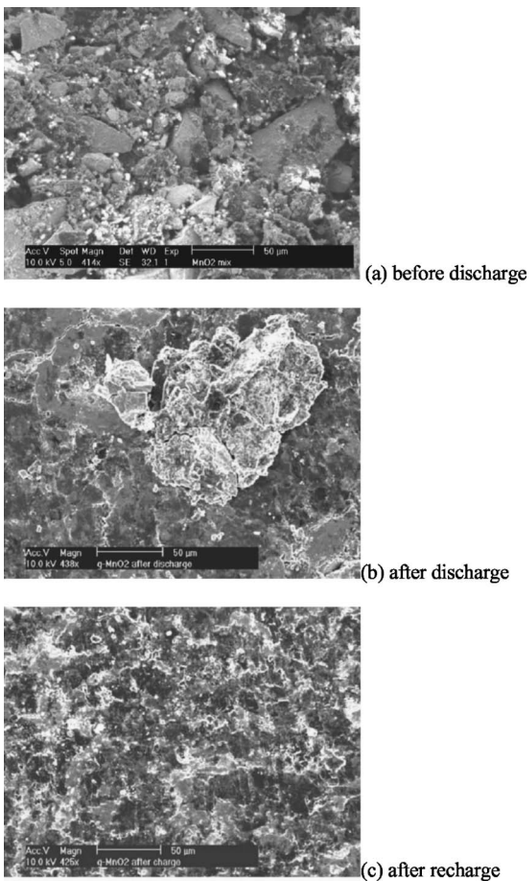

Figure 4. Scanning electron micrographs of MnO_2 cathode material.

thick layer of materials (like LiOH, Li_2CO_3, and H_2O) on the surface of the discharged products. The lithium carbonate is the result of LiOH electrolyte reacting with atmospheric carbon dioxide. Figure 5 and 6 show the XPS spectra of C (1s) and Li (1s) region of the discharged cathode MnO_2. As can be seen in Fig. 5, the Li_2CO_3 peak had a very strong signal before argon ion bombardment and then decreased in intensity on continuous etching of the surface layer, indicating that the Li_2CO_3 layer was removed. The hydrocarbon peak at 285 eV had a strong intensity before argon ion bombardment, whereas after 40 min and 1 h etching it decreased in intensity towards a lower binding energy of 284 eV. Figure 6 shows the XPS spectra of Li (1s) region. It can be seen in the figure that upon argon etching the peak corresponding to 55.6 eV starts to disappear. Instead, a new peak emerged at 54.7 eV. The intensity of the signal for the new peak at 54.7 eV remained fairly constant upon argon ion etching. Based upon binding energies as reported,[14,15] we assign the peak at 55.5 eV to Li_2CO_3 and the second peak at 54.7 eV to intercalated lithium. The basis of this assignment is that during the reduction process lithium has been intercalated into the MnO_2 cathode from aqueous LiOH solution. Hence, the XPS profiles of Fig. 5 and 6 show that Li is present in the carbonate layer as Li_2CO_3 and in MnO_2 as intercalated lithium.

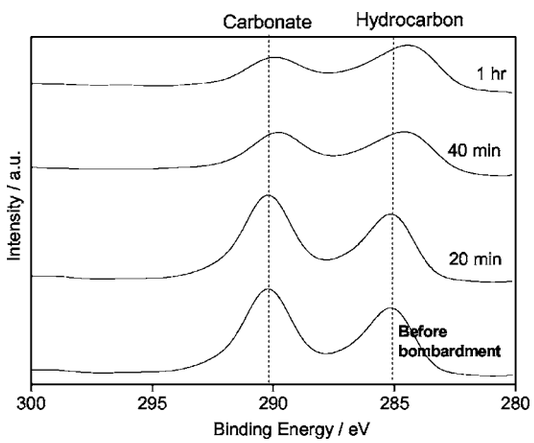

Figure 5. XPS spectra of C (1s) for the cathode MnO_2. Time in the figure indicates the ion beam sputtering duration.

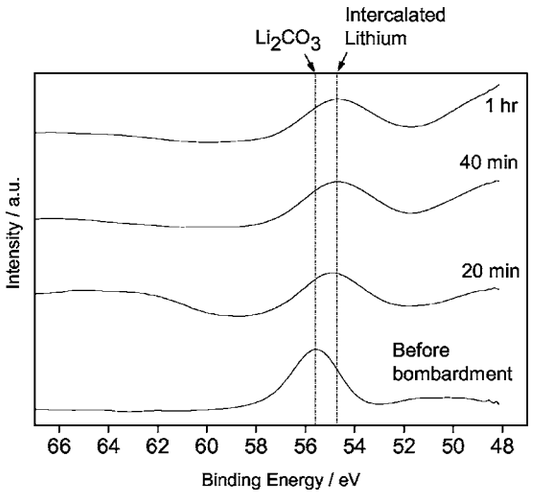

Figure 6. XPS spectra of Li (1s) for the cathode MnO_2. Time in the figure indicates the ion beam sputtering duration.

From the evidence based on the XPS depth profiles, it can be concluded that formation of Li_2CO_3 occurs on the cathode (MnO_2) surface, which inhibits the diffusion of OH^- but permits the Li^+ ion to undergo intercalation into the active layer of the γ-MnO_2 host material as shown in Eq. 2. This would provide an intercalation mechanism for a secondary aqueous cell.

Effect of TiS_2 additive in the MnO_2 cathode.— The influence of TiS_2 as an addition to manganese dioxide cathode on the performance of an aqueous lithium hydroxide electrolyte battery was investigated. This was motivated by studies which have shown the beneficial effects of Bi^{3+} and other ionic additions.[16-19] A potential candidate in this regard has been Ti^{4+} ion.[18] In this work, small amounts of TiS_2 as additives have been employed by physically mixing TiS_2 powder into the cathode and investigating the effects of this on the electrochemical behavior. In order to determine if there was any influence of this additive on the MnO_2 structure, SEM and XPS have been performed. The morphology of the surface of MnO_2 in the presence of various amounts of TiS_2 as additive is shown in Fig. 7. The SEM micrograph with the additive of the 5 wt % shows a little change in morphology, i.e., rounded particles around 10 μm in diameter. Apart from this no other information relating to structural changes can be drawn from SEM. Figure 8 shows the XPS spectra of the Mn 2p region for the γ-MnO_2 cathode material with various wt % of TiS_2 additive. For 1 and 3 wt % additive, two peaks corresponding to Mn $2p_{1/2}$ and 3/2 spin-orbit split components were observed. For the 3 wt % samples, peaks are well defined and are more intense that those of the 5 wt % material, where only a shoulder of peak is seen and shifted 1 eV towards lower binding energy. This shows that increasing the additive from 3 to 5 wt % alters the manganese state in MnO_2. Its corresponding infrared spectra analysis has been performed (not included here) and agrees well with the

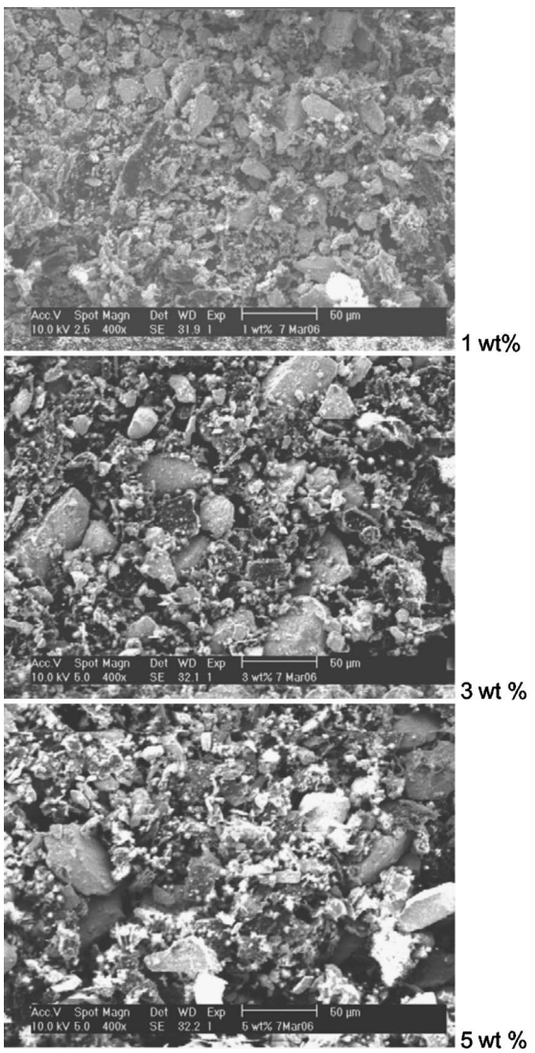

Figure 7. Scanning electron micrographs of the MnO_2 cathode in the presence of small amounts of TiS_2 additive.

XPS data. This suggests that the bonding of Mn in MnO_2 has been slightly altered by physically mixing it[18] with TiS_2 at higher weight loadings.

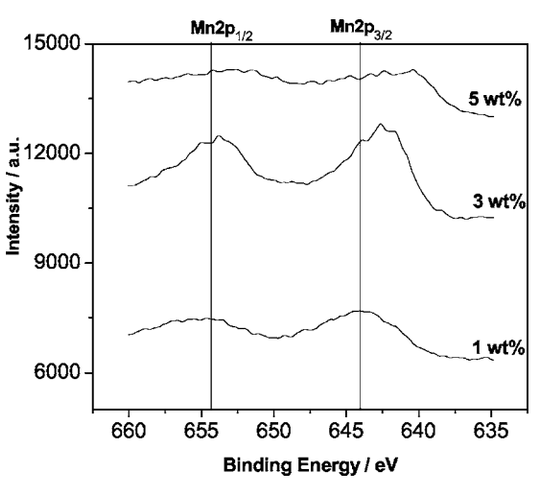

Figure 8. XPS spectra of Mn 2p for the MnO_2 cathode with TiS_2 additive.

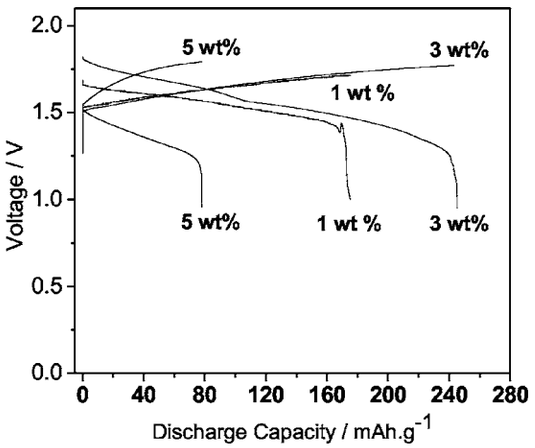

Figure 9. The first discharge-charge profiles of Zn-MnO_2 cells containing TiS_2 additive.

Figure 9 shows the performance of the MnO_2 cell as a function of TiS_2 loading. For the plain MnO_2 (without additive) the observed capacity is 150 mAh/g (from Fig. 1). With 1 wt % additive, there was an increase in capacity value from 150 to 175 mAh/g, although it is negligible. For a cell with 3 wt % additive, electrode capacity dramatically increased to 260 mAh/g, whereas, for a cell with 5 wt % additive, capacity decreased to 75 mAh/g. Although the shape of the discharge curve remains unchanged for the various wt %, the average voltage is significantly altered for 5 wt %. The cell could be reversibly discharged and charged, and a significant voltage polarization is seen for 5 wt % additive. The increase in discharge capacity could be explained in terms of the TiS_2 additive stabilizing the MnO_2 octahedra (as seen in Fig. 8) towards dimensional changes that occur during the discharge process.[18] However, increasing the additive content from 3 to 5 wt % causes a decrease in the cell voltage and capacity. This result is in accordance with the XPS and IR spectra revealing that the Mn state in MnO_2 is altered by physical mixing of additives.

The discharge curves for the first ten cycles illustrating the cyclability for 3 and 5 wt % additive are shown in Fig. 10 and 11, respectively. The cycling performance is quite good in 3 wt % without much irreversible capacity as seen for 5 wt % additive in Fig. 11. However, a slight inflection around 1.5 V is seen only for MnO_2 containing additive. Figure 12 compares the cycling performance of

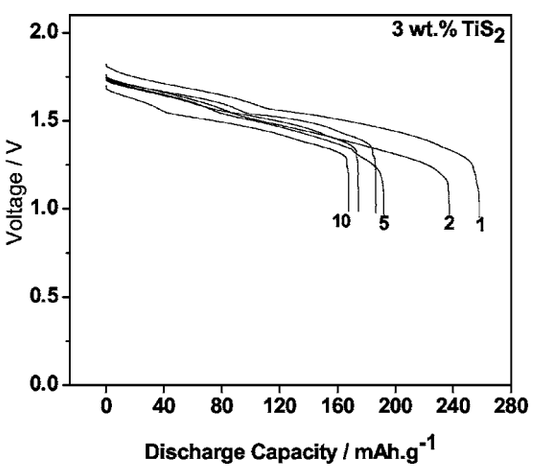

Figure 10. Discharge curves for various cycles illustrating the cyclability of MnO_2 containing 3 wt % additive.

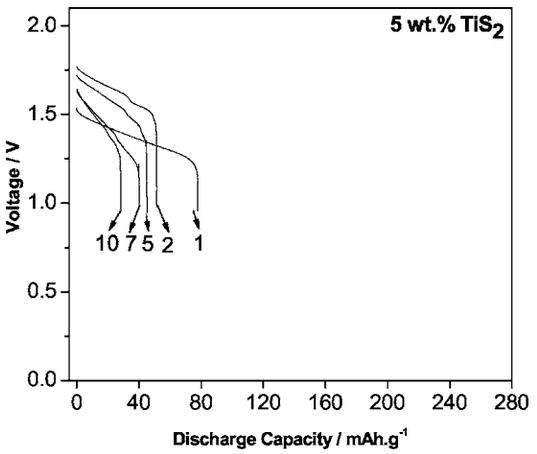

Figure 11. Discharge curves for various cycles illustrating the cyclability of MnO_2 containing 5 wt % additive.

the Zn-MnO_2 cells for the first ten cycles in the presence of 0, 3, and 5 wt % additive. The available capacity is low and decreases quickly for the 5 wt % additive. The plain MnO_2 cell shows significantly improved capacity, although this is still less than that of 3 wt % additive. The cell capacity for 3 wt % additive is high and decreased gradually for the first five cycles (from 260 to 192 mAh/g, reflecting a loss of 25%) then stabilized with a loss of only 13% at the tenth cycle. Although the plain MnO_2 shows improved capacity retention during cycling, its energy density is lower than that of 3 wt % additive.

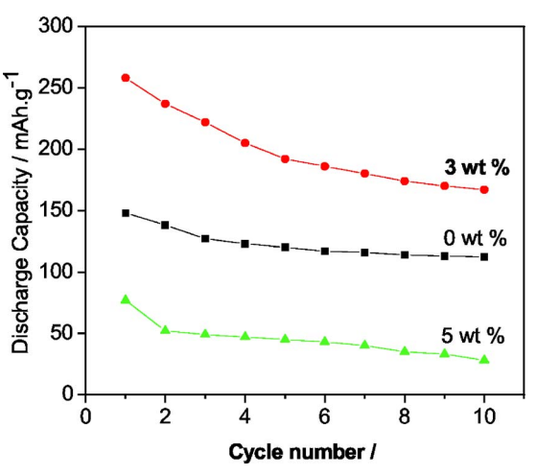

Figure 12. (Color online) Comparison of the discharge capacity vs cycle number for the Zn-MnO_2 cell in the presence of 0, 3, and 5 wt % additive.

Based upon the results discussed above, it can be concluded that at 3 wt % loading of the TiS_2 additive stabilizes the MnO_2 crystalline structure and this leads to a high cell capacity. At the highest weight loading (5 wt %) the crystalline structure is no longer stabilized by TiS_2 and the cell capacity decreases.

Conclusions

The characterization of the products formed when MnO_2 is discharged in a Zn-MnO_2 in aqueous LiOH cell indicates that the cell discharge mechanism involves Li^+ intercalation into the host structure. This is confirmed by analysis of the products formed on the discharged MnO_2 cathode by using SEM and XPS techniques. Small amounts of TiS_2 additive into the MnO_2 cathode improve the discharge capacity by stabilizing the structure of MnO_2. However, increasing the additive content above 3 wt % causes a decrease in the cell voltage and discharge capacity.

Acknowledgments

M.M. is grateful to Murdoch University for providing a Research Excellence Grant Scheme funding. The financial support of Australian Nuclear Science and Engineering (AINSE) under AINGRA 06248 for carrying out a part of the work at Australian Nuclear Science and Technology (ANSTO) is also acknowledged. M.M. would also like to thank Peter Fallon of Murdoch University for his technical support.

Murdoch University assisted in meeting the publication costs of this article.

References

1. M. Armand, in *Materials for Advanced Batteries*, D. W. Murphy, J. Broadhead, and B. C. H. Steele, Editors, p. 145, Plenum Press, New York (1980).
2. T. Ohzuku and A. Ueda, *J. Electrochem. Soc.*, **141**, 2972 (1994).
3. J. R. Dahn, U. von Sacken, H. Al Janaby, and M. K. Juzkow, *J. Electrochem. Soc.*, **138**, 2207 (1991).
4. N. Reimers, E. W. Fuller, E. Rossen, and J. R. Dahn, *J. Electrochem. Soc.*, **140**, 3396 (1993).
5. T. Ohzuku, M. Kitagawa, and T. Hirai, *J. Electrochem. Soc.*, **136**, 3169 (1989).
6. M. Manickam, K. Minato, and M. Takata, *J. Electrochem. Soc.*, **150**, 1085 (2003).
7. M. Manickam, *J. Power Sources*, **113**, 179 (2003).
8. A. K. Padhi, K. S. Nanjundaswamy, and J. B. Goodenough, *J. Electrochem. Soc.*, **144**, 1188 (1997).
9. M. Minakshi, P. Singh, T. B. Issa, S. Thurgate, and R. DeMarco, *J. Power Sources*, **130**, 254 (2004).
10. E. Levi, E. Zinigrad, H. Teller, M. D. Levi, and D. Aurbach, *J. Electrochem. Soc.*, **144**, 4133 (1997).
11. Y. S. Lee and M. Yoshio, *Electrochem. Solid-State Lett.*, **4**, 166 (2001).
12. M. Minakshi, P. Singh, T. B. Issa, S. Thurgate, and R. DeMarco, *J. Power Sources*, **153** 165 (2006).
13. F. C. Laman and K. Brandt, *J. Power Sources*, **24**, 195 (1998).
14. *Handbook of X-Ray Photoelectron Spectroscopy*, Physical Electronics Division, Perkin Elmer Corporation, Eden Prairie, MN (1992).
15. K. Kanamura, H. Tamura, S. Shiraishi, and Z. Takehara, *Electrochim. Acta*, **40**, 913 (1995).
16. S. W. Donne, G. A. Lawrence, and D. A. J. Swinkels, *J. Electrochem. Soc.*, **144**, 2954 (1997).
17. H. S. Wroblowa and N. Gupta, *J. Electroanal. Chem. Interfacial Electrochem.*, **238**, 93 (1987).
18. V. K. Nartey, L. Binder, and A. Huber, *J. Power Sources*, **87**, 205 (2000).
19. Y. F. Yao, N. Gupta, and H. S. Wroblowa, *J. Electroanal. Chem. Interfacial Electrochem.*, **223**, 107 (1987).